Temporal modulation instabilities of counterpropagating waves in a finite dispersive Kerr medium. II. Application to Fabry–Perot cavities

M. Yu and C. J. McKinstrie

Department of Mechanical Engineering and Laboratory for Laser Energetics, University of Rochester, Rochester, New York 14627

Govind P. Agrawal

The Institute of Optics, University of Rochester, Rochester, New York 14627

Absolute instabilities of counterpropagating pump beams in a dispersive Kerr medium, placed inside a Fabry–Perot cavity, are analytically studied by use of the analysis and the results of part I [J. Opt. Soc. B **14**, **607** (1998)]. Our approach allows characterization of such a complicated nonlinear system in terms of a doubly resonant optical parametric oscillator. We consider the growth of modulation-instability sidebands associated with each pump beam when weak probe signals are injected through one of the mirrors of the Fabry–Perot cavity. The results are used to obtain the threshold condition for the onset of the absolute instability and the growth rate for the unstable sidebands in the above-threshold regime. As expected, the well-known Ikeda instability is recovered at low modulation frequencies. The effects of the group-velocity dispersion are found to become quite important at high modulation frequencies. Although the absolute instability dominates in the anomalous-dispersion regime, it exists even in the normal-dispersion regime of the nonlinear medium. Below the instability threshold, our analysis provides analytic expressions for the probe transmittivity and the reflectivity of the phase-conjugated signal that is generated through a four-wave-mixing process. © 1998 Optical Society of America [S0740-3224(98)04102-2]

OCIS codes: 190.0190, 190.3270, 120.2230, 270.3100.

1. INTRODUCTION

The nonlinear interaction between counterpropagating waves in a finite Kerr medium has been studied extensively.[1–5] In part I of this set of two papers,[6] we developed a theoretical model to study the instabilities of counterpropagating waves in a finite, dispersive, Kerr medium and showed how the effects of boundary reflections can be included. At high modulation frequencies for which the effects of group-velocity dispersion (GVD) are important, the results can be interpreted in terms of an analogy to a highly detuned, distributed feedback (DFB) laser[7] (except that photon pairs corresponding to the two spectral sidebands are involved). We showed in part I (referred to hereinafter as Ref. 6) that the problem can be further simplified by a classification of the parameter space in terms of the relative importance of the DFB and boundary reflections. In practice, a finite Kerr medium can be considered a Fabry–Perot (FP) cavity whose mirror reflectivities are large enough that the DFB effects can be neglected compared with the boundary effects. Thus the problem becomes analogous to a doubly resonant FP parametric oscillator,[8] except that one must consider the signal and idler pairs at the sideband frequencies simultaneously. Such an approach is well suited for the investigation of the GVD effects on the Ikeda instability in a nonlinear FP cavity.

The objective of this paper is to provide a detailed study of this important case. After a brief review of the relevant results of Ref. 6, the case of cw pump waves counterpropagating in a FP cavity that contains a dispersive Kerr medium is investigated theoretically in Section 2 by studying the medium response to a weak probe beam. The threshold condition for the absolute instability and the growth rates of the unstable modes are obtained in Section 3. The transmission and reflection coefficients of the probe are calculated and analyzed in Section 4. Although a silica fiber is used as an example, the results are applicable to any dispersive Kerr medium.

2. THEORETICAL ANALYSIS

The equations used to model the system, the underlying assumptions, and the technique used to solve them have been discussed in Ref. 6 and need not to be repeated here. The new feature is that the nonlinear medium is placed inside a FP cavity. We assume for simplicity that the nonlinear medium occupies the entire length l of the FP cavity. The evolution of two counterpropagating pump waves is described by a set of two coupled nonlinear Schrödinger equations [see Ref. 6, Eqs. (1) and (2)]. The counterpropagating cw pump fields in the medium are represented by the steady-state solutions of these equations, given by

$$A_{1s}(t, z) = A_{10} \exp[i\gamma(|A_{10}|^2 + 2|A_{20}|^2)z], \qquad (1)$$

$$A_{2s}(t, z) = A_{20} \exp[i\gamma(|A_{20}|^2 + 2|A_{10}|^2)(l - z)]. \qquad (2)$$

Here γ is the nonlinear coefficient, k_0 is the linear wave number, and the complex constants $A_{10} = |A_{10}|\exp(i\phi_{10})$ and $A_{20} = |A_{20}|\exp(i\phi_{20})$ refer to the amplitudes of the counterpropagating pump waves.

To study the stability of the steady-state solution, we inject weak probe fields into the cavity and look at the response of the system. With the same notation as in Ref. 6, the weak probe fields inside the cavity can be written as

$$\delta A_1(t, z) = \overline{\delta A}_1(t, z) \exp[i\gamma(|A_{10}|^2 + 2|A_{20}|^2)z], \qquad (3)$$

$$\delta A_2(t, z) = \overline{\delta A}_2(t, z) \exp[i\gamma(|A_{20}|^2 + 2|A_{10}|^2)(l - z)]. \qquad (4)$$

Their evolution in the frequency domain is described by Eq. (52) of Ref. 6 in terms of $\delta A_1(\omega, z)$ and $\delta A_2(\omega, z)$, which are the Fourier transforms of $\overline{\delta A}_1(t, z)$ and $\overline{\delta A}_2(t, z)$, respectively. For completeness, we reproduce Eq. (52) of Ref. 6 here:

$$\begin{bmatrix} \delta\mathbf{A}_1(\omega, z) \\ \delta\mathbf{A}_2(\omega, z) \end{bmatrix} = \exp(i\beta_1\omega z)\begin{bmatrix} \mathbf{M}_f(\omega, z) \\ \mathbf{M}_{fb}(\omega, z) \end{bmatrix}\mathbf{c}_f$$
$$+ \exp[i\beta_1\omega(l - z)]\begin{bmatrix} \mathbf{M}_{bf}(\omega, l - z) \\ \mathbf{M}_b(\omega, l - z) \end{bmatrix}\mathbf{c}_b, \qquad (5)$$

where the vectors $\delta\mathbf{A}_1$ and $\delta\mathbf{A}_2$ are formed by use of the two forward-propagating and two backward-propagating sidebands, respectively. Each pair of sidebands consists of Fourier components at the frequencies ω and $-\omega$. Thus $\delta\mathbf{A}_j(\omega, z) = [\delta A_j(\omega, z), \delta A_j^*(-\omega, z)]$ is a column vector with the two elements representing sideband amplitudes ($j = 1, 2$). The matrix elements for all matrices appearing in Eq. (5) are given in Section 3 of Ref. 6.

We obtained Eq. (5) by linearizing the nonlinear Schrö-dinger equations and using the small-parameter analysis in terms of a small parameter ϵ. To define the dimensionless parameter ϵ, we introduce several characteristic lengths and frequencies. The walk-off length and the dispersion length at a given modulation frequency ω are defined as $l_W = (\beta_1\omega)^{-1}$ and $l_D = (\beta_2\omega^2)^{-1}$, where β_1, β_2 are the inverse of group velocity and the GVD coefficient, respectively. Assuming that the pump–power ratio $S \equiv |A_{20}|^2/|A_{10}|^2 \leq 1$ (without loss of generality), we define the nonlinear length at a given power $P = |A_{10}|^2$ as $l_N = (\gamma P)^{-1}$. We further define $\omega_W = \gamma P/\beta_1$ and $\omega_D = (\gamma P/\beta_2)^{1/2}$ to represent the modulation frequencies at which the walk-off length and the dispersion length, respectively, become equal to the nonlinear length. For modulation frequencies far below ω_W the effects of walk-off are not important. Similarly, for modulation frequencies far below ω_D the GVD effects become negligible. With these definitions, the parameter

$$\epsilon = \omega_W/\omega_D = \sqrt{|\beta_2|\gamma P/\beta_1^2}, \qquad (6)$$

is a small quantity even for materials with a relatively large GVD coefficient and at relatively high power levels since, in practice, the GVD effects are negligible simply when the walk-off length is comparable to the nonlinear length. In this paper, as well as in Ref. 6, the dispersive and nonlinear effects are of main concern. We thus introduce a normalized modulation frequency $\Omega = \omega/\omega_D$ and a normalized length $L = l/l_N$. The GVD effect is negligible when $\Omega \ll 1$, and the Kerr medium can be treated as dispersionless by setting $\beta_2 = 0$ (see Ref. 6, Section 2 for more details).

By treating ϵ as a small parameter, we concluded in Ref. 6 that the cross matrices $\mathbf{M}_{fb}$ and $\mathbf{M}_{bf}$ in Eq. (5) can be ignored when $\Omega \gg \epsilon$ (or $\omega \gg \omega_W$) and the amplitude-reflection coefficients of the FP-cavity mirrors are much larger than $O(\epsilon/\Omega)$. When the first condition is satisfied, the forward- and backward-propagating pairs of sidebands evolve independently as if the counterpropagating pump wave were absent. The role of the counterpropagating pump wave is to induce a weak scattering of the propagating sidebands through cross-phase modulation in the opposite direction. This scattering can be considered as a weak DFB of the magnitude $O(\epsilon/\Omega)$ and can be neglected when FP reflection coefficients are $\gg O(\epsilon/\Omega)$.

When $\omega \leq \omega_W$ [i.e., $\Omega \leq O(\epsilon)$], the above discussion indicates that the GVD effects are negligible. This dispersionless case has been studied before.[1] In this paper, we concentrate on the case $\Omega \gg \epsilon$. As has been pointed out in Ref. 6, for very small values of ϵ, there can be a region, $1 \gg \Omega \gg \epsilon$ that overlaps with the two cases considered in this paper and Ref. 1. In this region, the frequency is low enough that dispersion is not important, and yet high enough that DFB is weak. Normally, the cavity-mirror feedback is much stronger than the DFB so that the second condition is easily satisfied. This is true even for weak reflections such as those occurring at the uncoated air–glass interface of an optical fiber having an amplitude-reflection coefficient of $\sim$0.2 (4% power reflectivity).

Using silica fiber as an illustrative example,[9] let us assume a power of $P = 10$ W, a nonlinear coefficient of $\gamma = 10$ W^{-1} km^{-1}, a group velocity of $1/\beta_1 = 0.2$ mm/ps, and a GVD coefficient of $|\beta_2| = 20$ ps^2/km. Then $l_N \sim 10$ m, and ϵ is only $\sim 10^{-5}$. Further, the frequencies ω_W and ω_D are ~ 20 μs^{-1} (or 3 MHz) and 2 ps^{-1} (or 0.3 THz), respectively.

A. Sideband Amplitudes

As discussed above, we can generally neglect the effects of DFB inside the Kerr medium placed in a FP cavity. This observation simplifies the analysis considerably since by ignoring the cross matrices in Eq. (5), the evolution of each pair of sidebands can be studied independently. In fact, one can use the transfer matrices $\mathbf{M}_f(\omega, l)$ and $\mathbf{M}_b(\omega, l)$ for the sidebands of the two pump beams individually, and write the solutions in the form

$$\delta\mathbf{A}_1(\omega, l) = \exp(i\beta_1\omega l)\mathbf{M}_f(\omega, l)\delta\mathbf{A}_1(\omega, 0), \qquad (7)$$

$$\delta\mathbf{A}_2(\omega, 0) = \exp(i\beta_1\omega l)\mathbf{M}_b(\omega, l)\delta\mathbf{A}_2(\omega, l). \qquad (8)$$

The transfer matrix for the modulation-instability (MI) sidebands of an individual pump is well known,[10] and the two matrices $\mathbf{M}_f(\omega, l)$ and $\mathbf{M}_b(\omega, l)$ are given by Eqs. (34)

and (35) of Ref. 6 in terms of Y_1, Y_2, $r_{1\pm}$, and $r_{2\pm}$. Since $r_{m+} = r_{m-}$ ($m = 1, 2$), if the pump phase is assumed to be zero, we drop the subscript $\pm$ on r_1 and r_2. For completeness, we give here expressions of Y_1 and r_1:

$$Y_1(\omega) = \sqrt{(\beta_2\omega^2/2 + \gamma|A_{10}|^2)^2 - (\gamma|A_{10}|^2)^2}, \quad (9)$$

$$r_1(\omega) = (Y_1 - \beta_2\omega^2/2)/(\gamma|A_{10}|^2) - 1. \quad (10)$$

Similar expressions hold for the counterpropagating pump beam.

It is easy to show that $|\mathbf{M}_f| = 1$, and the transfer matrix establishes a one-to-one correspondence between the input and output amplitudes of the coupled sidebands. Note also that $\mathbf{M}_f^2(\omega, l) = \mathbf{M}_f(\omega, 2l)$ as required on a physical basis. Similar expressions and properties hold for $\mathbf{M}_b$. In analogy to a FP laser, the behavior of $\mathbf{M}_f(\omega, l)$ along the distance l gives the information on the evolution of the coupled sidebands inside the cavity. As has been pointed out in Ref. 6, its magnitude can either increase linearly or exponentially, providing a linear or exponential gain for the coupled sidebands. The latter case occurs in the anomalous-dispersion regime only when $\Omega \sim (2)^{1/2}$, while the former happens whenever $|Y_1|l \ll 1$, translating into the requirement of $\Omega \ll 1$ (i.e., dispersionless propagation) in both the normal and the anomalous regimes. Similar conditions apply to $\mathbf{M}_b$.

B. Effects inside the Fabry–Perot Cavity

We now proceed to include the effects of mirror reflections occurring inside the FP cavity on the single-pass solution given by Eqs. (7) and (8). If the probe fields $\delta\mathbf{A}_i(\omega)$ are injected at the left mirror located at $z = 0$, the boundary conditions require that

$$\delta\mathbf{A}_1(\omega, 0) = \mathbf{T}_f'\delta\mathbf{A}_i(\omega) + \mathbf{R}_f\delta\mathbf{A}_2(\omega, 0), \quad (11)$$

$$\delta\mathbf{A}_2(\omega, l) = \mathbf{R}_b\delta\mathbf{A}_1(\omega, l), \quad (12)$$

where

$$\mathbf{R}_j = \begin{bmatrix} r_j \exp(i\psi_{rj}) & 0 \\ 0 & r_j \exp(-i\psi_{rj}) \end{bmatrix} \quad (j = f, b),$$

$$\mathbf{T}_f' = \begin{bmatrix} t_f' \exp(i\phi_{t'f}) & 0 \\ 0 & t_f' \exp(-i\phi_{t'f}) \end{bmatrix}.$$

Here, $\psi_{rf} = \phi_{rf} + \Delta_2$ and $\psi_{rb} = \phi_{rb} + \Delta_1$ with $\Delta_1 = k_0l + \gamma(|A_{10}|^2 + 2|A_{20}|^2)l$, and $\Delta_2 = k_0l + \gamma(|A_{20}|^2 + 2|A_{10}|^2)l$ are the propagation constants associated with the pump waves. Further, $r_f \exp(i\phi_{rf})$ and $r_b \exp(i\phi_{rb})$ are the reflection coefficients for the left and right mirrors ($0 < r_f < 1$ and $0 < r_b < 1$,) respectively, and $t_f' \exp(i\phi_{t'f})$ is the transmission coefficient into the medium at the left mirror. Although we assume that the cavity mirrors are in contact with the Kerr medium, a similar treatment can be applied when the mirrors are located away from the Kerr medium. Equations (11) and (12) are the same as Eqs. (53) and (54) of Ref. 6 if we set $\delta\mathbf{A}_i = 0$. The simplification made by neglecting the cross matrices allows us to consider the general case of nonzero injection in our analytical study.

From Eqs. (7), (8), (11), and (12), the probe field inside the cavity is related to the input as

$$\delta\mathbf{A}_1(\omega, 0) = [1 - \exp(2i\beta_1\omega l)\mathbf{R}_f\mathbf{M}_b\mathbf{R}_b\mathbf{M}_f]^{-1}\mathbf{T}_f'\delta\mathbf{A}_i(\omega), \quad (13)$$

where, and in the following, $\mathbf{M}_f(\omega, l)$ and $\mathbf{M}_b(\omega, l)$ have been shortened to $\mathbf{M}_f$ and $\mathbf{M}_b$ to simplify the notation. This equation is a coupled-sidebands version of a similar equation relating the input and the output fields in an FP cavity in which the vectors and matrices become scalar quantities.

An absolute instability occurs when the field inside the cavity $\delta\mathbf{A}_1(\omega, 0)$ can build up from noise even in the absence of external injection $\delta\mathbf{A}_i(\omega)$. Such instabilities can be studied by solving the eigenvalue problem

$$[1 - \exp(2i\beta_1\omega l)\mathbf{R}_f\mathbf{M}_b\mathbf{R}_b\mathbf{M}_f]\delta\mathbf{A}_1(\omega, 0) = 0 \quad (14)$$

in the complex ω plane. The frequencies at which an absolute instability occurs are found by setting the determinant

$$D(\omega) = |1 - \exp(2i\beta_1\omega l)\mathbf{R}_f\mathbf{M}_b\mathbf{R}_b\mathbf{M}_f| = 0. \quad (15)$$

Multiple solutions for ω represent different longitudinal "supermodes" of the system, with the real and imaginary part providing the frequency and growth (or damping) rate of each supermode. Therefore an absolute instability occurs whenever Eq. (15) permits solutions with $\mathrm{Im}(\omega) > 0$. This can happen above certain pump power. The eigenvectors give the longitudinal supermodes for the doubly resonant FP parametric oscillator.

Below the absolute-instability threshold, our general solution can be used to obtain the reflected and transmitted fields through the FP cavity containing a dispersive Kerr medium by using the relations

$$\delta\mathbf{A}_t(\omega) = \mathbf{T}_b\delta\mathbf{A}_1(\omega, l), \quad \delta\mathbf{A}_r(\omega) = \mathbf{T}_f\delta\mathbf{A}_2(\omega, 0), \quad (16)$$

where

$$\mathbf{T}_j = \begin{bmatrix} t_j \exp(i\phi_{tj}) & 0 \\ 0 & t_j \exp(-i\phi_{tj}) \end{bmatrix}, \quad (j = f, b),$$

and $t_f \exp(i\phi_{tf})$ and $t_b \exp(i\phi_{tb})$ are the transmission coefficients out of the medium for the front boundary and rear boundary, respectively. By use of Eqs. (7), (8), (11), and (12), the transmitted and reflected fields are related to the input field as

$$\delta\mathbf{A}_t(\omega) \equiv \mathbf{T}\delta\mathbf{A}_i(\omega),$$

$$= \exp(i\beta_1\omega l)\mathbf{T}_b\mathbf{M}_f$$

$$\times (1 - \exp(i2\beta_1\omega l)\mathbf{R}_f\mathbf{M}_b\mathbf{R}_b\mathbf{M}_f)^{-1}\mathbf{T}_f'\delta\mathbf{A}_i(\omega), \quad (17)$$

$$\delta\mathbf{A}_r(\omega) \equiv \mathbf{R}\delta\mathbf{A}_i(\omega),$$

$$= \exp(i2\beta_1\omega l)\mathbf{T}_f\mathbf{M}_b\mathbf{R}_b\mathbf{M}_f(1 - \exp(i2\beta_1\omega l)$$

$$\times \mathbf{R}_f\mathbf{M}_b\mathbf{R}_b\mathbf{FM}_f)^{-1}\mathbf{T}_f'\delta\mathbf{A}_i(\omega), \quad (18)$$

where $\mathbf{T}$ and $\mathbf{R}$ are defined as the transmission and reflection matrices for the nonlinear FP system. They satisfy the symmetry relations between $-\omega$ and ω so that $T_{21} = T_{12}^*$, $T_{22} = T_{11}^*$, $R_{21} = R_{12}^*$, and $R_{22} = R_{11}^*$. Physically T_{11} and T_{12} indicate the transmission coefficients at the input frequency and at the four-wave-mixing frequency, respectively.

3. ABSOLUTE INSTABILITY

We now proceed to describe the absolute instability of a FP cavity containing a dispersive Kerr medium. The calculation of $D(\omega)$ from Eq. (15) is straightforward, resulting in

$$D(\omega) = 1 - r_f r_b \exp(i2\beta_1 \omega l)G(\omega)$$
$$+ [r_f r_b \exp(i2\beta_1 \omega l)]^2 = 0, \qquad (19)$$

where

$$G(\omega) = M_{f11}M_{b11} \exp[i(\psi_{rf} + \psi_{rb})]$$
$$+ M_{f21}M_{b12} \exp[i(\psi_{rf} - \psi_{rb})] + \text{c.c.} \quad (20)$$

Equation (19) can be recast in a familiar form of the threshold condition for a laser,

$$r_f r_b G_{\pm}^{\text{eff}}(\omega)\exp(2i\beta_1 \omega l) = 1, \qquad (21)$$

where the effective gain is defined as

$$G_{\pm}^{\text{eff}}(\omega) = (G \pm \sqrt{G^2 - 4})/2. \qquad (22)$$

Since $G_{+}^{\text{eff}}G_{-}^{\text{eff}} = 1$, either $G_{+}^{\text{eff}} \geq 1$ or $G_{-}^{\text{eff}} \geq 1$. For an unstable supermode, the gain should overcome the loss, i.e.,

$$|G_{\pm}^{\text{eff}}(\omega)| > 1/(r_f r_b). \qquad (23)$$

For $r_f r_b \ll 1$, $|G_{\pm}^{\text{eff}}| \gg 1$ is needed for instability, which in turn requires $|G| \gg 1$. In this case, Eq. (22) simplifies to yield $G_{+}^{\text{eff}} \approx G$, while G_{-}^{eff} can be neglected. In the following, we use the convention that the subscript $+$ denotes the branch with higher gain. Under this convention, $\ln|G_{+}^{\text{eff}}| = -\ln|G_{-}^{\text{eff}}| \geq 0$, and the net gain $g(\omega)$ used in Ref. 6 is simply $r_f r_b G_{+}^{\text{eff}}(\omega)$.

To gain some physical insight, let us start with the special case of equal pump powers ($|A_{10}| = |A_{20}|$) so that $Y_1 = Y_2$, $r_1 = r_2$. By expressing the transfer matrices in terms of Y_1, Y_2, r_1, and r_2, Eq. (20) becomes

$$G = (\exp[i(2Y_1 l + \psi_{rf} + \psi_{rb})]$$
$$\times \{1 - r_1^2\exp[-i2(\psi_{rf} + \psi_{rb})]\}$$
$$+ \exp[-i(2Y_1 l + \psi_{rf} + \psi_{rb})]$$
$$\times \{1 - r_1^2 \exp[i2(\psi_{rf} + \psi_{rb})]\})/(1 - r_1^2)$$
$$+ 2[\cos(\theta_f - \theta_b) - \cos(\psi_{rf} + \psi_{rb})]$$
$$\times (\gamma|A_{10}|^2 l)^2 \text{ sinc}^2(Y_1 l), \qquad (24)$$

where $\theta_f = \psi_{rf} + \phi_{20} - \phi_{10}$, $\theta_b = \psi_{rb} + \phi_{10} - \phi_{20}$, and $\text{sinc}(x) = \sin x/x$. When $\psi_{rf} + \psi_{rb}$ and $\theta_f - \theta_b$ are multiples of 2π, G in Eq. (24) is considerably simplified and Eq. (22) becomes

$$G_{\pm}^{\text{eff}} = \exp(\mp i2Y_1 l). \qquad (25)$$

This equation has a very simple physical meaning if we note that $-iY_1$ is just the gain from MI in the case of anomalous dispersion, and Y_1 is imaginary with a maximum magnitude of $\gamma|A_{10}|$.[9]

In the normal-dispersion regime, $\beta_2 \geq 0$, and Y_1 is real. Thus Eq. (21), when combined with Eq. (25), does not have solutions with Im $\omega \geq 0$, and the system is stable. However, in the case of anomalous dispersion ($\beta_2 < 0$), the MI gain can overcome the reflection loss, and the system can become unstable. This instability

does not correspond to the conventional Ikeda instability in a FP cavity since it does not exist for dispersionless medium. Figure 1(a) shows the gain spectra of MI for $\beta_2 < 0$ by plotting $\ln|G_{+}^{\text{eff}}|$ as a function of the normalized frequency for two values of the normalized length L.

We determine the frequencies and the growth rates for different unstable supermodes by using Eq. (25) in Eq. (21) and solving for Ω the following relation:

$$\exp\{iL[2\Omega/\epsilon \mp \sqrt{s(\Omega^2/2 + 1)^2 - 1}]\} = 1/(r_f r_b), \qquad (26)$$

where $s = \text{sign}(\beta_2) = \pm 1$ and $\epsilon = (|\beta_2|\gamma|A_{10}|^2/\beta_1^2)^{1/2}$ is the small quantity introduced in Eq. (6). This equation can be solved by treating ϵ as a small parameter. In a typical case in which $1 - r_f r_b$ is not a small quantity we come to the conclusion that mode spacing is so small that $\Omega_r \equiv \text{Re }\Omega$ varies almost continuously within the MI gain spectrum. The growth rate $\Omega_i \equiv \text{Im }\Omega$ is a small quantity and is given by

$$\Omega_i = \epsilon[\ln|\exp[\pm iL \sqrt{s(\Omega_r^2/2 + 1)^2 - 1}]|$$
$$+ \ln(r_f r_b)]/(2L). \qquad (27)$$

In terms of physical units, this equation can be written as

$$\omega_i = [\ln|G_{+}^{\text{eff}}(\omega_r)| + \ln(r_f r_b)]/(2l\beta_1). \qquad (28)$$

Apparently, the mode spacing is $O(\epsilon) \ll 1$, while the scale of variation of the gain curves is $O(1)$ in the normalized frequency.

Although the above conclusions are drawn under the special case of equal pump powers with $\psi_{rf} + \psi_{rb}$ and $\theta_f - \theta_b$ being multiples of 2π, they are valid in general since a similar analysis can be applied. Thus the gain spectrum $|G_{+}^{\text{eff}}(\omega_r)|$ gives almost all the needed information. According to Eq. (28), the gain has to exceed the cavity loss $-\ln(r_f r_b) > 0$ for an instability to occur, and their difference determines the growth or damping rate of each supermode. The threshold condition around frequency ω_r is $\ln|G_{+}^{\text{eff}}(\omega_r)| \geq -\ln(r_f r_b)$. The other branch of the gain curve, $\ln|G_{-}^{\text{eff}}|$, is always below threshold (it is actually below zero). The growth or damping rate is on the scale of $1/(2l\beta_1)$, which is $\sim 10 \ \mu\text{s}^{-1}$ if we use $l = 1/(\gamma P)$ as a typical value and use the values of Section 2 for γ, P, and β_1. For these parameters, the gain varies on the scale of $2 \ \text{ps}^{-1}$, and the mode spacing is on the scale of $10 \ \mu\text{s}^{-1}$. Generally, the mode spacing is $\sim\omega_W$, and the growth rate varies on the scale of ω_D.

To show how the MI gain changes with unequal pump powers, Figs. 1(b)–1(d) show the gain spectra by use of Eqs. (22) and (20) for unequal pump intensities and different values of the phases. Multiple gain regions are due to the constructive or destructive interference effects induced by the nonlinear phase shifts. The three horizontal loss lines represent the mirror loss $-\ln(r_f r_b)$ for $r_f r_b = 4\%$ (upper line), 30% (middle line) and 50% (lower line). The difference between the gain curve and the loss line indicates the growth rate of the sideband amplitudes in units of $1/(2l\beta_1) = \omega_W/(2L)$. As expected, as the mirror loss is reduced by increasing the mirror reflectivities, the MI sidebands grow more rapidly because of the increased feedback.
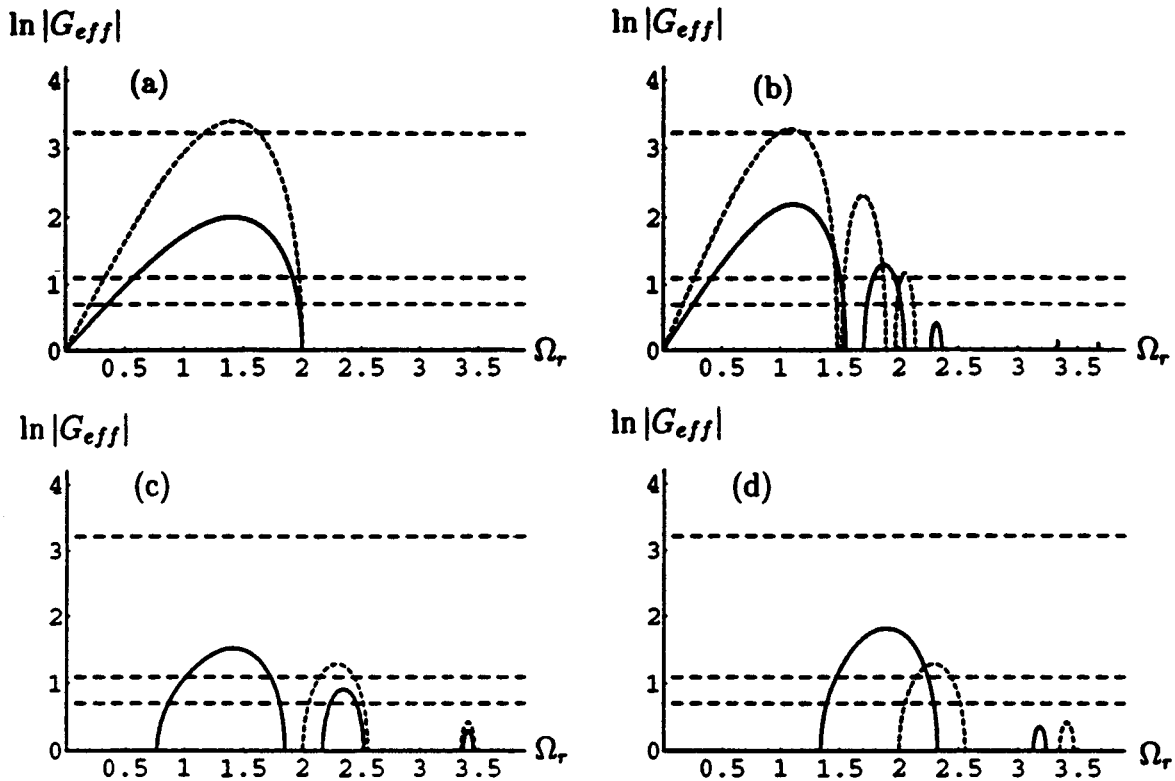
Fig. 1. Gain spectra of modulation instability in the case of anomalous dispersion obtained by plotting $\ln|G^{\text{eff}}(\Omega_r)|$ as a function of Ω_r. (a) Pump–power ratio $S = |A_{20}|^2/|A_{10}|^2 = 1$, and $\psi_{rf} + \psi_{rb}$, $\phi_{20} - \phi_{10}$, and $\psi_{rf} - \psi_{rb}$ are multiples of 2π. $L = l\,\gamma|A_{10}|^2 = 1$ and $L = 1.7$ for the solid and dashed curves, respectively. (b) Same as (a) except that $S = 1/3$, and the solid and the dashed curves are for $L = 1.7$ and 2.6, respectively. (c) Same as (a) except that $L = 1$, and the solid and the dashed curves are for $\phi_{20} - \phi_{10} = \pi/4$ and $\pi/2$, respectively. (d) Same as (a) except that $L = 1$, and the solid and the dashed curves are for $\psi_{rf} + \psi_{rb} = \pi/2$ and π, respectively. In all cases, the three horizontal loss lines represent the mirror loss $-\ln(r_f r_b)$ for $r_f r_b = 4\%$ (upper line), 30% (middle line), and 50% (lower line).

The absolute instability can exist even in the normal-dispersion regime of a dispersive Kerr medium. This instability has its origin in the feedback provided by the mirrors of a FP cavity and is analogous to the Ikeda instability. Figure 2 shows the gain spectra for $\beta_2 > 0$ for several different parameter combinations. From the discussion of Section 2, it should be noted that the gain-curve picture does not apply around the zero-modulation frequency within a bandwidth covering several ω_W. In this region, the results from the dispersionless treatment[1] indicate that the growth rate in the presence of the Ikeda instability can vary on the scale of mode spacing. However, the high-frequency limit of the dispersionless treatment can still be described by the method used here and corresponds to our gain curve at the low-frequency end. In fact, the low-frequency limits of the gain curves in Fig. 2(b) correspond to the Ikeda instability. The same is true for the highest gain curves in Figs. 2(a) and 2(c). There is no correspondence to the conventional Ikeda instability for the rest of gain curves shown in Figs. 1 and 2, where the instabilities are due solely to the presence of the dispersive effects.

Since $G_+^{\text{eff}} \approx G$ can be used for large gain, Eq. (24) indicates that large pump powers or long Kerr media (or both) are needed. In such a limit, the MI gain contributes most to the gain curve in the anomalous-dispersion re-gime because of its exponential dependence on both parameters. In fact, it can be shown that

$$G_+^{\text{eff}} \approx G$$
$$= \{\exp(-iY_2 l)[r_1 r_2 \exp(i\theta_f)$$
$$\quad - \exp(-i\theta_f)][r_1 r_2 \exp(i\theta_b) - \exp(-i\theta_b)]$$
$$\quad - \exp(iY_2 l)[r_1 \exp(i\theta_f) - r_2 \exp(-i\theta_f)]$$
$$\quad \times [r_1 \exp(i\theta_b) - r_2 \exp(-i\theta_b)]\}$$
$$\quad \times \exp(-iY_1 l)/[(1 - r_1^2)(1 - r_2^2)], \qquad (29)$$

for the gain curve around its peak, where we have neglected $\exp(iY_1 l) = \exp(-|Y_1|l)$ compared with $\exp(-iY_1 l)$. We have kept $\exp(\mp iY_2 l)$ since Y_2 can either be imaginary or real within the frequency range $0 < \Omega_r < 2$, where Y_1 is purely imaginary. In the large-gain limit in the normal-dispersion case, however, the gain value at the low-frequency end increases at most quadratically (due to the double-pass nature) with both of the parameters.

For a dispersionless Kerr medium, the results of this section reduce to those obtained previously by Firth,[1] who studied this special case in 1981. When GVD is included but the feedback effects are removed by setting the mirror
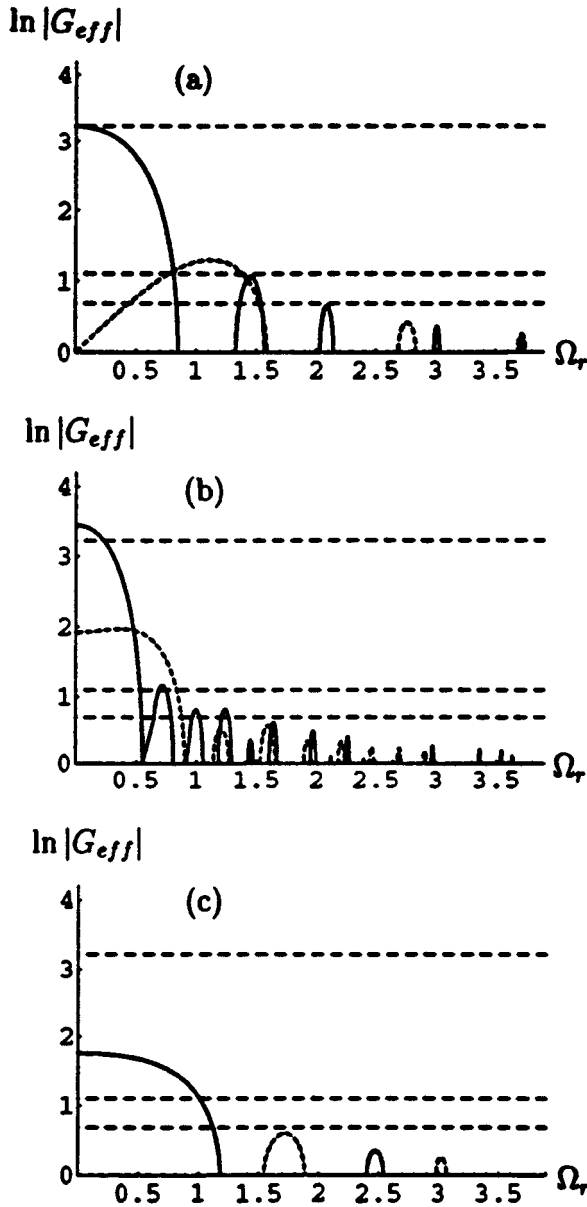
Fig. 2. Gain spectra of modulation instability in the case of normal dispersion. (a) Pump–power ratio $S = |A_{20}|^2/|A_{10}|^2 = 1$, the phases $\psi_{rf} + \psi_{rb}$ and $\psi_{rf} - \psi_{rb}$ are multiples of 2π, and $\phi_{20} - \phi_{10} = \pi/2$. The dashed and the solid curves are for $L = 1$ and 2.6, respectively. (b) Same as (a) except that $S = 1/3$, and the dashed and the solid curves are for $L = 2.6$ and 5, respectively. (c) Same as (a) except that $L = 1$, $\psi_{rf} + \psi_{rb} = \pi/2$, and the dashed and the solid curves are for $\phi_{20} - \phi_{10} = 0$ and $\pi/2$ respectively. In all cases, the three horizontal loss lines are the same as in Fig. 1.

reflectivities to zero, our results reduce to those of Law and Kaplan,[4] as discussed in Ref. 6.

4. PROBE TRANSMISSIVITY AND REFLECTIVITY

In pump–probe types of experiments, an external probe, shifted from the pump frequency by ω, is injected into the cavity together with the counterpropagating pump beams, and information about the nonlinear system is

gathered by measuring probe transmissivity and reflectivity below the instability threshold of the system. The transmission and reflection matrices can be calculated in a straightforward manner from Eqs. (17) and (18), and the results are given by

$$T_{11}(\omega) = \exp[i(\beta_1\omega l + \phi_{tb} + \phi_{t'f})]t_b t_f'\{M_{f11} - r_f r_b$$
$$\times \exp[i(2\beta_1\omega l - \psi_{rf} - \psi_{rb})]M_{b22}\}/D(\omega), \tag{30}$$

$$T_{12}(\omega) = \exp[i(\beta_1\omega l + \phi_{tb} - \phi_{t'f})]t_b t_f'\{M_{f12} + r_f r_b$$
$$\times \exp[i(2\beta_1\omega l + \psi_{rf} - \psi_{rb})]M_{b12}\}/D(\omega), \tag{31}$$

$$R_{11}(\omega) = \exp[i(2\beta_1\omega l + \phi_{tf} + \phi_{t'f})]t_f t_f' r_b$$
$$\times \{\exp(-i\psi_{rb})M_{f21}M_{b12} + \exp(i\psi_{rb})M_{f11}M_{b11}$$
$$- \exp[i(2\beta_1\omega l - \psi_{rf})]r_f r_b\}/D(\omega), \tag{32}$$

$$R_{12}(\omega) = \exp[i(2\beta_1\omega l + \phi_{tf} - \phi_{t'f})]t_f t_f' r_b$$
$$\times [\exp(-i\psi_{rb})M_{f22}M_{b12}$$
$$+ \exp(i\psi_{rb})M_{f12}M_{b11}]/D(\omega), \tag{33}$$

together with $T_{21} = T_{12}^*$, $T_{22} = T_{11}^*$, $R_{21} = R_{12}^*$, and $R_{22} = R_{11}^*$.

There are two frequency scales over which the transmission and reflection coefficients vary with frequency. In the normalized variables Ω and L, the fast scale of Ω is in the term $\exp(i2\beta_1\omega l) \equiv \exp(i2\Omega L/\epsilon)$, resulting in $O(\epsilon)$-scale oscillations corresponding to mode spacing. The other terms in Eqs. (30)–(33) and (19) depend on frequency on the $O(1)$ scale. The behavior on both scales can be studied independently.

Considerable simplification occurs for the case in which $r_f r_b \ll 1$. In this limit, Eqs. (30)–(33) become

$$T_{11}(\omega) = \exp[i(\beta_1\omega l + \phi_{tb} + \phi_{t'f})]t_b t_f' M_{f11}/$$
$$\times [1 - r_f r_b \exp(i2\beta_1\omega l)G], \tag{34}$$

$$T_{12}(\omega) = \exp[i(\beta_1\omega l + \phi_{tb} - \phi_{t'f})]t_b t_f' M_{f12}/$$
$$\times [1 - r_f r_b \exp(i2\beta_1\omega l)G], \tag{35}$$

$$R_{11}(\omega) = \exp[i(2\beta_1\omega l + \phi_{tf} + \phi_{t'f})]t_f t_f' r_b$$
$$\times [\exp(-i\psi_{rb})M_{f21}M_{b12}$$
$$+ \exp(i\psi_{rb})M_{f11}M_{b11}]/[1 - r_f r_b$$
$$\times \exp(i2\beta_1\omega l)G], \tag{36}$$

$$R_{12}(\omega) = \exp[i(2\beta_1\omega l + \phi_{tf} - \phi_{t'f})]t_f t_f' r_b$$
$$\times [\exp(-i\omega_{rb})M_{f22}M_{b12}$$
$$+ \exp(i\psi_{rb})M_{f12}M_{b11}]/[1 - r_f r_b$$
$$\times \exp(i2\beta_1\omega l)G]. \tag{37}$$

It is easy to see that the frequency response of these coefficients consists of fast oscillations at the mode spacing determined by the term $\exp(i2\beta_1\omega l)$ in the denominator while the upper and lower bounds are determined by setting the denominator to $1 \mp r_f r_b|G(\omega)|$, respectively.
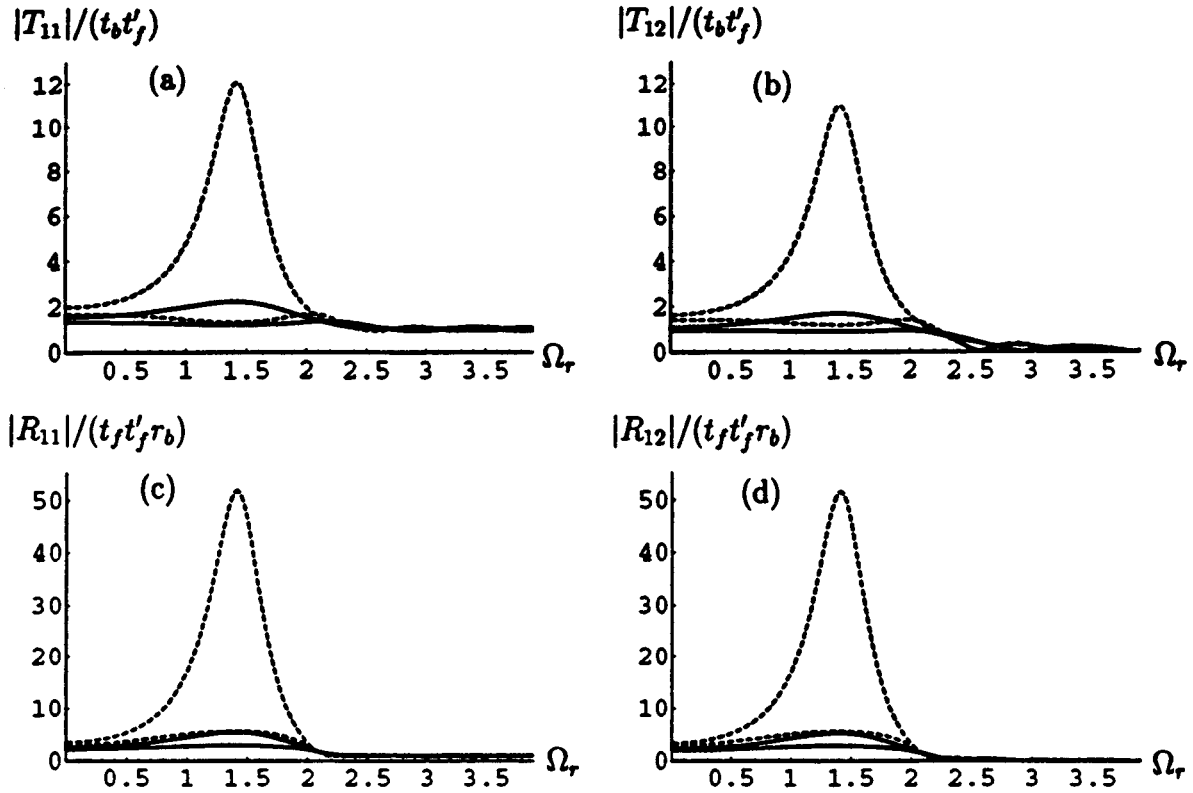
Fig. 3. The transmissivity and reflectivity of an external probe plotted as a function of the pump–probe detuning. Only the upper and lower envelopes, associated with fast oscillations on the scale of mode spacing, are shown for a FP cavity with $r_f r_b = 4\%$. The solid and dashed curves are for $L = 1$ and $L = 1.5$, respectively. Other parameters are the same as in Fig. 1(a). (a) Probe transmissivity; (b) transmissivity of the four-wave-mixing frequency component; (c) probe reflectivity; and (d) reflectivity of the four-wave-mixing frequency component.

Figure 3 shows the upper and lower bounds of the frequency response of these coefficients by plotting $|T_{11}(\omega)|/(t_b t_f')$, $|T_{12}(\omega)|/(t_b t_f')$, $|R_{11}(\omega)|/(t_f t_f' r_b)$, and $|R_{12}(\omega)|/(t_f t_f' r_b)$ for the case $r_f r_b = 4\%$. As the instability threshold is approached, the upper bound goes to infinity, resulting in large amplification of the probe field.

It should be noticed that A_{10} and A_{20} refer to the steady-state fields inside the cavity, which are related to the input pump fields A_{1i} and A_{2i} outside the cavity by the boundary conditions

$$A_{10} = A_{1i} t_f' \exp(i\phi_{t'f}) + A_{20} \exp(il\Delta_2) r_f \exp(i\phi_{rf}), \tag{38}$$

$$A_{20} = A_{2i} t_b' \exp(i\phi_{t'b}) + A_{10} \exp(il\Delta_1) r_b \exp(i\phi_{rb}). \tag{39}$$

These relations can be used to calculate A_{1i} and A_{2i} from A_{10} and A_{20}, or vice versa. The multistability nature of this type of equation has been studied extensively[11,12] and is not the main focus here. When the boundary reflections are relatively weak, $A_{10} = A_{1i} t_f' \exp(i\phi_{t'f})$ and $A_{20} = A_{2i} t_b' \exp(i\phi_{t'b})$, where we have assumed $|A_{2i}|t_b' r_f \ll |A_{1i}|t_f'$, $|A_{1i}|t_f' r_b \ll |A_{2i}|t_b'$, and $r_f r_b \ll 1$.

5. CONCLUSIONS

The main objective of this paper has been to study analytically the effects of GVD on the stability of a nonlinear FP cavity. For this purpose, we have concentrated on the

modulation frequency range for which the walk-off length is much larger than the nonlinear length. For the perturbative fields propagating inside the cavity, the DFB induced by the counterpropagating pumps waves is often negligible compared with the localized feedback at cavity mirrors. The system behavior is then governed by the coupling of copropagating sidebands and the boundary reflections. Such a nonlinear system can be interpreted in terms of a doubly resonant parametric oscillator, with the signal and idler fields playing the role of coupled sidebands in our model. This physically transparent model allows the complicated nonlinear system to be characterized in a simple and familiar language.

Absolute instabilities are found to occur in both the normal- and the anomalous-dispersion regimes and are described by the gain spectra plotted as a function of the modulation frequency. The discrete supermode frequencies likely to become unstable are almost continuously distributed under the gain curve. The analytical expressions are derived for both the growth rate and the frequency of various supermodes. For each unstable supermode, there are generally two sidebands (corresponding to the signal and idler fields in the language of parametric oscillators), which beat to cause pulsing in the output intensity. While the instability at low modulation frequencies corresponds to the conventional Ikeda instability, new instability regions are found owing to the finite dispersion of the Kerr medium. For high pump powers or large medium lengths, the instability in the anomalous-

dispersion regime is driven by the MI gain because of the exponential dependence of the MI gain on these parameters. In the normal-dispersion regime, the contribution of the Kerr or four-wave-mixing effects to the gain depends at most quadratically on these parameters. In the absence of GVD, our results reduce to those previously obtained by Firth.[1] When GVD is included but the feedback effects are removed by setting the mirror reflectivities to zero, our results reduce to those of Law and Kaplan,[4] as discussed in Ref. 6.

Below threshold, we studied the transmission and reflection characteristics of the nonlinear system for a weak probe. The transmitted and reflected beams appear not only at the original frequency of the probe but also at the phase-conjugate (or idler) frequency owing to the coupling between them induced by the nonlinear process of four-wave-mixing. The transmission and reflection coefficients are analytically obtained. Their frequency response consists of fast oscillations at the mode spacing of the nonlinear system with an envelope slowly varying on the same scale as the gain curve. As the threshold approaches, the amplitude of the envelope goes to infinity, resulting in large amplification.

ACKNOWLEDGMENTS

REFERENCES

1. W. J. Firth, Opt. Commun. **39**, 343 (1981).
2. Y. Silberberg and I. Bar-Joseph, J. Opt. Soc. Am. B **1**, 662 (1984).
3. W. J. Firth and C. Paré, Opt. Lett. **13**, 1096 (1989); W. J. Firth, C. Paré, and A. FitzGerald, J. Opt. Soc. Am. B **7**, 1087 (1990).
4. C. T. Law and A. E. Kaplan, Opt. Lett. **14**, 734 (1989); J. Opt. Soc. Am. B **8**, 58 (1991).
5. W. J. Firth and C. Penman, Opt. Commun. **94**, 183 (1992).
6. M. Yu, C. J. McKinstrie, and G. P. Agrawal, J. Opt. Soc. Am. B **14**, 607 (1998).
7. G. P. Agrawal and N. K. Dutta, *Semiconductor Lasers*, 2nd ed. (Van Nostrand Reinhold, New York, 1993), Chap. 7.
8. Y. R. Shen, *The Principles of Nonlinear Optics* (Wiley, New York, 1984), Chap. 9.
9. G. P. Agrawal, *Nonlinear Fiber Optics*, 2nd ed. (Academic, San Diego, Calif., 1995).
10. M. Yu, G. P. Agrawal, and C. J. McKinstrie, J. Opt. Soc. Am. B **12**, 1126 (1995), and references therein.
11. R. W. Boyd, *Nonlinear Optics* (Academic, Boston, 1992).
12. H. M. Gibbs, *Optical Bistability: Controlling Light with Light* (Academic, Orlando, Fla., 1985).